Intracellular protein interaction mapping with FRET hybrids

Xia You*, Annalee W. Nguyen*†, Abeer Jabaiah*, Mark A. Sheff‡, Kurt S. Thorn‡§, and Patrick S. Daugherty*¶

*Department of Chemical Engineering, University of California, Santa Barbara, CA 93106; and ‡Bauer Center for Genomics Research, Room 208, Harvard University, 7 Divinity Avenue, Cambridge, MA 02138

Edited by Jack W. Szostak, Massachusetts General Hospital, Boston, MA, and approved October 14, 2006 (received for review June 28, 2006)

A quantitative methodology was developed to identify protein interactions in a broad range of cell types by using FRET between fluorescent proteins. Genetic fusions of a target receptor to a FRET acceptor and a large library of candidate peptide ligands to a FRET donor enabled high-throughput optical screening for optimal interaction partners in the cytoplasm of *Escherichia coli*. Flow cytometric screening identified a panel of peptide ligands capable of recognizing the target receptors in the intracellular environment. For both SH3 and PDZ domain-type target receptors, physiologically meaningful consensus sequences were apparent among the isolated ligands. The relative dissociation constants of interacting partners could be measured directly by using a dilution series of cell lysates containing FRET hybrids, providing a previously undescribed high-throughput approach to rank the affinity of many interaction partners. FRET hybrid interaction screening provides a powerful tool to discover protein ligands in the cellular context with potential applications to a wide variety of eukaryotic cell types.

cell sorting | protein–ligand interactions

The ability to identify and quantitatively characterize protein–protein interactions in living cells is essential for developing a detailed, system-level understanding of cellular function. The yeast two-hybrid (Y2H) system has served as the primary genetic tool to discover potential biological interaction partners for an enormous number of proteins (1, 2). Application of Y2H assays to each of the nearly 6,000 yeast ORFs enabled construction of the first large-scale protein interaction network in yeast (3, 4), and similar interaction studies were performed subsequently in *Drosophila melanogaster* and *Caenorhabditis elegans* (5, 6). Human–protein interaction networks are less well characterized and present difficult challenges to interaction mapping approaches. In fact, only a small fraction of an estimated 10^5 to 10^6 human–proteome interactions (7) have been unambiguously identified, primarily by using Y2H and mass spectrometry approaches (7, 8). Unfortunately, high-throughput Y2H assays are typically prone to a high frequency of false positives that complicate the interpretation of interaction data. In some studies, it has been estimated that >50% of putative interactions identified are false positives (9).

Several important challenges remain in the elucidation of protein–protein interaction networks and their influence on cell function (10). Large-scale interaction maps can portray basic network structure but lack quantitative features needed to understand network function. A predictive understanding of network function likely will require the elucidation of equilibrium and kinetic properties within a network, including individual equilibrium-binding constants. Furthermore, existing high-throughput approaches (e.g., Y2H) are not well suited to investigate real-time dynamics in protein networks essential for understanding cell function (11) because detection, in these cases, is based on a nonreversible process. Additionally, new approaches are needed to identify interacting partners in compartments other than the nucleus, such as within the cytosol or at membrane surfaces (12). In some cases, it also would be desirable to screen for interactions directly in the context of a specific animal or plant cell type. Finally, because many proteins are composed of several unique protein-interaction domains (13), it can be difficult to match interaction partners to specific, spatially segregated domains on the target protein. Such domain-level mapping information would aid in developing a more detailed picture of protein network structure that accounts for competitive or cooperative interactions. Given these problems, new high-throughput approaches are needed to detect, screen, and quantitatively characterize intracellular protein interactions.

The use of genetically encoded fluorescent proteins that exhibit FRET is especially attractive to investigate protein interactions in living cells because these interactions can be detected in a wide variety of cell types and compartments (14–16), in near real-time, enabling investigation of dynamic behavior (17, 18). But, importantly, the relatively small FRET dynamic range provided by fluorescent proteins has limited their application to probing known and putative interacting partners (19), rather than screening libraries to discover new interaction partners. We recently reported the evolutionary design of a pair of fluorescent proteins (CyPet and YPet) with a substantially expanded dynamic range for intracellular FRET measurements (20). Using this new FRET probe, we sought to develop a quantitative, high-throughput protein interaction assay that enables direct detection and screening of libraries for protein-interaction partners to identify and map protein interactions in a wider variety of living cells. The utility of this approach was demonstrated by screening large peptide libraries for ligands that specifically recognize two target receptors in bacteria. Moreover, we demonstrated that protein–ligand interactions can be detected in the cytoplasm of both yeast and mammalian cells with greatly enhanced sensitivity, enabling high-throughput interaction screening in the cellular context.

Results

Analysis of Known Interaction Partners by Using FRET Hybrids. To enable quantitative protein-interaction screening, a general strategy was developed involving intracellular coexpression of a target receptor and a library of ligands as fusion proteins with FRET-optimized yellow and cyan fluorescent proteins, YPet and CyPet (20), respectively (Fig. 1). Given the expanded dynamic range of these probes, we anticipated that library screening could be accomplished with FACS and that the

Author contributions: X.Y., A.W.N., A.J., M.A.S., K.S.T., and P.S.D. designed research; X.Y., A.W.N., A.J., and M.A.S. performed research; X.Y. and A.W.N. contributed new reagents/analytic tools; X.Y., A.W.N., and A.J. analyzed data; and X.Y., A.W.N., K.S,T., and P.S.D. wrote the paper.

The authors declare no conflict of interest.

This article is a PNAS direct submission.

Abbreviation: Y2H, yeast two-hybrid.

†Present address: Applied Biosystems, 2130 Woodward Street, Austin, TX 78744-1832.

§Present address: University of California, San Francisco MC2140, Genentech Hall Room S252, 600 16th Street, San Francisco, CA 94158-2517.

¶To whom correspondence should be addressed. E-mail: psd@engineering.ucsb.edu.

www.pnas.org/cgi/doi/10.1073/pnas.0605422103

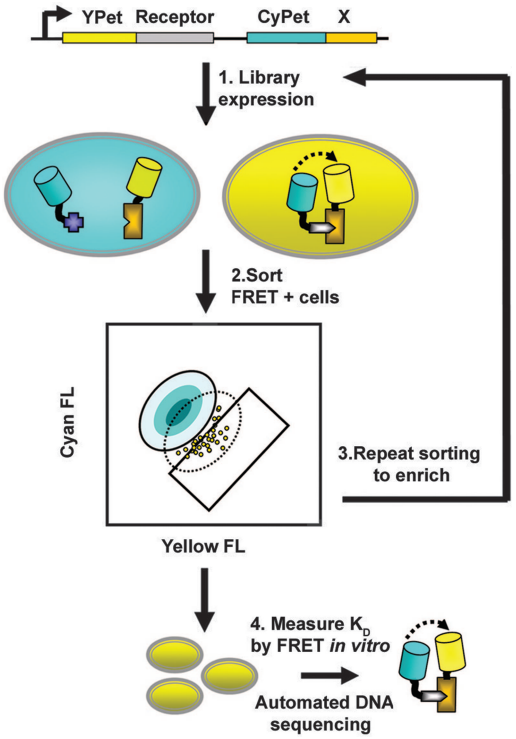

Fig. 1. Protein-interaction screening with FRET hybrids. Libraries of YPet-target receptor and CyPet-peptide fusions are expressed from a bicistronic expression vector (*1*), and cells exhibiting FRET are detected and sorted by FACS (*2*), amplified by growth, and enriched with additional cycles of FACS (*3*). Individual clones are isolated by sorting into 96-well plates, and the affinity of the YPet-target, CyPet–peptide interaction is determined directly by cell lysis and dilution (*4*).

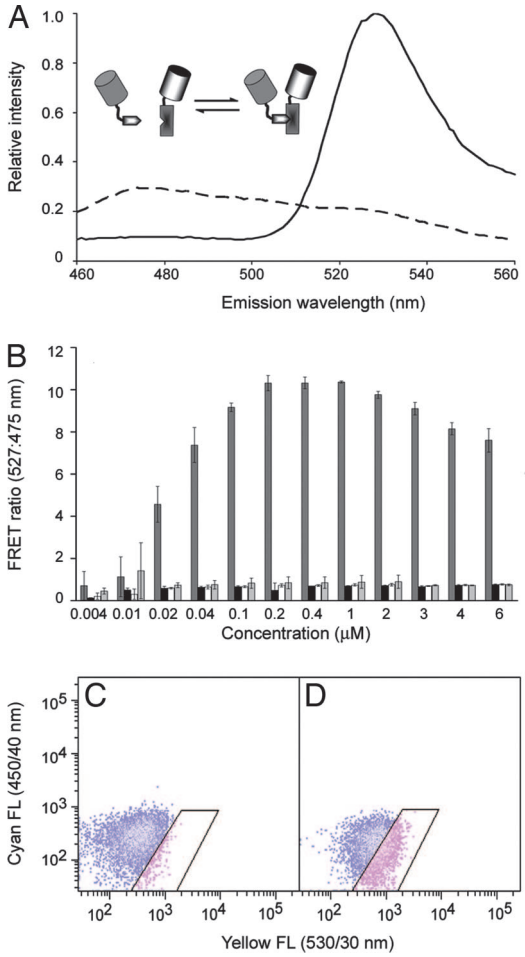

Fig. 2. Detection of receptor-ligand (FRET hybrid) interactions *in vitro* and *in vivo*. (*A*) Relative emission spectra of interacting partners (YPet-Mona+CyPet-P2, solid line) and noninteracting partners (YPet-Mona plus CyPet, dashed line) at 1 μM protein *in vitro*. (*B*) Ratiometric FRET signal of serially diluted mixtures of interacting partners YPet-Mona + CyPet-P2 (dark gray bars), or noninteracting partners: CyPet plus YPet (black), CyPet plus YPet-Mona (white), and CyPet-P2 plus YPet (light gray). (*C* and *D*) Fluorescence distributions of *E. coli* cell populations expressing noninteracting hybrids YPet-Mona plus CyPet (*C*) or interacting partners YPet-Mona plus CyPet-P2 (*D*) as measured by flow cytometry.

binding affinity of discovered interaction partners could be directly quantified by fluorimetry (Fig. 1). To validate this approach, a model interaction pair was chosen consisting of the C-terminal SH3 domain from monocytic adaptor protein (21) (hereafter referred to as Mona) and a high-affinity peptide ligand known as P2 (K_D = 100–200 nM) (22). The structure of the Mona–P2 complex has been determined by crystallography to 1.7-Å resolution, and the ligand preferences of Mona have been characterized extensively (22–24). Mona was genetically fused to the C terminus of YPet (YPet-Mona), and P2 was similarly tethered to CyPet (CyPet-P2) to create fluorescent fusion proteins capable of FRET (FRET hybrids) upon complex formation. To achieve appropriate intracellular stoichiometry for FRET, the FRET hybrids were expressed from a regulated, bicistronic expression vector. The maximum FRET dynamic range between free and bound hybrids was determined for mixtures of YPet-Mona and CyPet-P2 *in vitro* by using fluorimetry (Fig. 2 *A* and *B*). These interacting partners exhibited strong FRET (i.e., emission ratio of 527 nm: 475 nm) at total concentrations above the reported dissociation constant ($K_D \approx 100$ nM) and decreased FRET upon serial dilution (Fig. 2*B*), indicating that the Mona–P2 interaction is reversible. At the same time, three different pairings of noninteracting hybrids (CyPet plus YPet; CyPet plus YPet-Mona; CyPet-P2 plus YPet) did not exhibit increased FRET signals (Fig. 2*B*). Remarkably, the maximum FRET signal for interacting partners increased 14-fold over that obtained with noninteracting partners (Fig. 2*B*), a dynamic range substantially greater than that observed by using nonoptimized fluorescent protein FRET pairs to detect protein interactions (25–27). These results demonstrated that the YPet-Mona/CyPet-P2 interaction could be specifically detected by using FRET hybrids in complex cell lysates when using FRET-optimized probes CyPet and YPet.

FACS is ideally suited for screening large cellular libraries for differences in FRET resulting from protein interactions but requires that target and nontarget cells in the library population possess sufficiently different FRET signals. To maximize the dynamic range in *Escherichia coli*, the total intracellular concentration of FRET hybrids was adjusted by optimizing the duration of induction, and the resulting cell fluorescence was measured by flow cytometry. FRET was apparent in cells expressing interacting partners YPet-Mona and CyPet-P2, which exhibited increased yellow and reduced cyan fluorescence relative to cells expressing the noninteracting pair CyPet and YPet-Mona (Fig. 2 *C* and *D*). The maximum resolution between target cells (expressing interacting pairs) and nontarget cells (expressing noninteracting pairs) as measured by FACS was achieved with an induction period of 2–3 h (Fig. 5, which is published as supporting information on the PNAS web site). These results indicated that the FRET dynamic range between target and nontarget cells was sufficient for quantitative interaction screening by FACS.

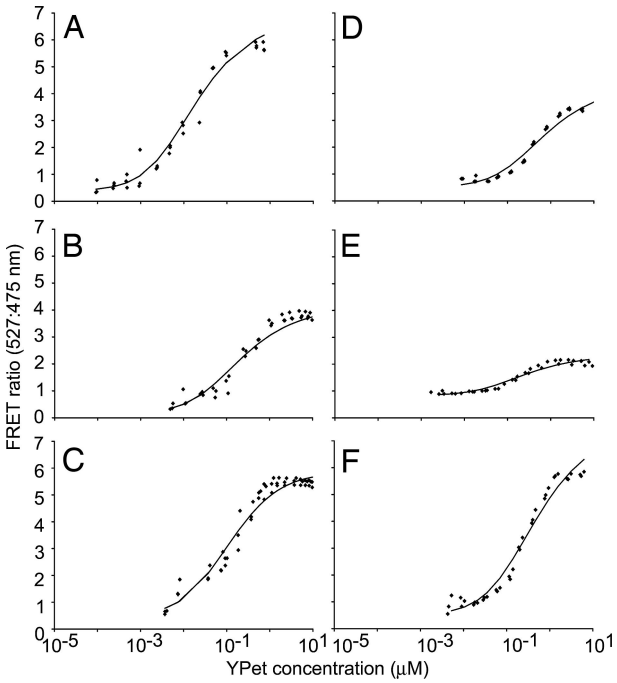

Fig. 3. Direct measurement of equilibrium dissociation constants of FRET hybrids. Measurement of the fluorescence ratios of individual isolated clones after cell lysis and serial dilution yielded equilibrium dissociation curves for YPet-Mona plus CyPet-P2 (*A*), YPet-Mona plus CyPet-MONA-2 (*B*), YPet-Mona plus CyPet-MONA-1 (*C*), YPet-PDZ2 plus CyPet-NR2 (*D*), YPet-PDZ2 plus CyPet-PDZ2-2 (*E*), and YPet-PDZ2 plus CyPet-PDZ2-4 (*F*). Triplicate FRET measurements were fit to an equilibrium-binding equation to determine relative K_D values.

FRET-Based Screening for Ligands Binding to Protein-Interaction Domains. We then investigated whether FRET hybrids would enable identification of optimal peptide ligands for two types of widely occurring protein-interaction modules: the C-terminal SH3 domain from Mona (22) and the second PDZ domain from postsynaptic density protein PSD-95 (28) (PDZ2). Combinatorial 15-mer peptide libraries, composed of 2×10^6 members, were constructed as C-terminal fusions to CyPet (CyPet-peptide) in bicistronic expression vectors that contained a gene encoding the target-domain fused to YPet. After transformation into *E. coli*, the target receptor and peptide ligand FRET hybrids were coexpressed in the cytoplasm (Fig. 1). Given the overlapping FRET signals between target and nontarget cells (in *E. coli*) (Fig. 2 *C* and *D*), target cells were enriched gradually by repeated sorting (Fig. 1). The leading edge of the cell population was collected, amplified by growth, and resorted. For each of the target domains, four cycles of FACS enabled enrichment of a cell population exhibiting increased FRET (Fig. 6, which is published as supporting information on the PNAS web site), similar to that observed for the Mona–P2 control interaction (Fig. 2 *C* and *D*).

To rank the relative ligand affinities in the context of cellular protein mixtures, apparent equilibrium dissociation constants were determined by measuring FRET signals for a dilution series of cell lysates. Each dilution series was fit with an equilibrium-binding isotherm (Fig. 3), enabling calculation of an apparent dissociation constant (Table 1), despite varying maximum FRET signals. With this ranking method, the K_D of the Mona–P2 interaction was determined to be ≈10 nM, ≈10- to 20-fold lower than that determined by using isothermal titration calorimetry (22). Similarly, a known PDZ binding peptide, derived from the C terminus of the NMDA receptor NR2 subunit (29, 30), exhibited a K_D 3-fold lower than that obtained by using fluorescence polarization (30) (Table 1).

Table 1. Protein-binding ligands identified with FRET hybrids

Clone	Sequence	K_D, nM
MONA SH3C		
SLP76-P2 (+)	PA**P**SID**R**ST**K**PPL	10
MONA-1	TSTP**P**LC**PPR**SA**K**AKVAKLGCFGG	90
MONA-2	ER**P**NR**PAR**EF**K**FRCP	100
MONA-3	SA**P**AR**PPR**TELPDLR	150
MONA-4	STAPAVC**R**LS**K**RCVR	360
MONA-5	VAP**P**PT**P**LWLY**R**DLP	500
MONA-6	YCRSNSAVP**P**PL**PPK**	620
MONA-7	VTSRGFS**P**KR**PPR**LS	>1,000
Consensus	**P**xx**PPR**xx**K**	
MONA-8	LLVMGFRHILG	100
PSD-95 PDZ2		
SESKE (−)	SE**S**KE	ND
NR2 (+)	IE**S**D**V**	340
Cript (+)	KQ**T**S**V**	290
PDZ2-1	PAISVNRPPSYS**T**P**V**	100
PDZ2-2	LAAMGFSHSALN**T**S**V**	110
PDZ2-3	RS**T**V**V**	200
PDZ2-4	PSAPHVTAMRY**WT**S**V**	230
PDZ2-5	VVW**WT**V**V**	250
PDZ2-6	SPTCLFESFPV**WT**M**V**	290
PDZ2-7	SVPLG**S**A**V**	290
PDZ2-8	SLTSEAQMSLR**WT**L**V**	400
PDZ2-9	PSGFPVTLMSVS**S**L**V**	480
PDZ2-10	SYDLSSCSPPS**WT**L	490
PDZ2-11	RSMPA**WT**VI	>1,000
PDZ2-12	PFPGGSLGHPH**WT**VL	>1,000
PDZ2-13	SLA**WS**S**V**	>1,000
PDZ2-14	PSHPPH**WS**DL	>1,000
PDZ2-15	VPI**WS**YIP	>1,000
PDZ2-16	MAI**WS**HL	>1,000
PDZ2-17	SAAI**WS**RC	>1,000
PDZ2-18	WLLIFDLPVNLLRLC	>1,000
Consensus	xx**WT**x**V**	

ND, not determined.

Identified Mona binders had apparent K_D values that ranged from 90 nM to >1 μM (Table 1). Importantly, although the P2 peptide possesses an exceptionally high affinity for Mona (22), most SH3 domain ligands exhibit K_D values that range from 100 nM to 200 μM (31), in agreement with the K_D values reported in Table 1. Because K_D values determined by using FRET in cell lysates were lower (i.e., higher apparent affinity) than those measured by using either isothermal titration calorimetry or fluorescence polarization, we also determined the K_D for selected FRET hybrids after purification from cell lysates. Interestingly, dissociation constants measured for purified Mona-P2 (170 nM) and PDZ2-NR2 (400 nM) were in close agreement (i.e., within 2-fold) with the values determined by using isothermal titration calorimetry and fluorescence polarization, respectively. Thus, FRET hybrid affinity measurements for purified proteins differed from those obtained in the presence of cellular protein. Regardless, affinity measurement in the presence of cell lysate protein by using FRET hybrids provided a simple and high-throughput approach to directly rank ligand affinity in the context of cellular protein.

Distinct ligand preferences were identified by using FRET hybrids for each of the target domains (Table 1). Mona binding ligands MONA-1, 2 3, 6, and 7, shared a strong consensus of PxxPPR/K, a known class II motif (PxxPxR/K) (31). Mona-binding ligands contained one or more characteristic SH3 bind-

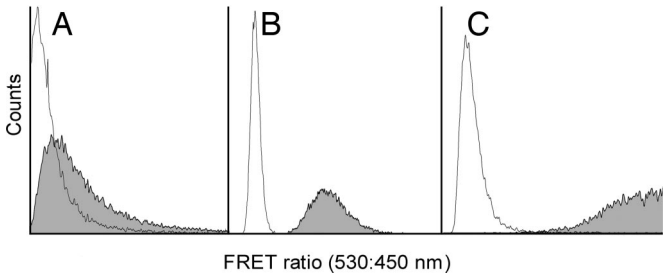

Fig. 4. FRET signals in bacteria, yeast, and mammalian cells. Ratiometric FRET signals for interacting (YPet-Mona plus CyPet-P2, filled) or noninteracting (YPet-Mona plus CyPet, open) hybrids in *E. coli* (*A*), *S. cerevisiae* (*B*), and human embryonic kidney cells (*C*) as measured by flow cytometry. Data is presented on a linear plot.

ing motifs, including PxxxRxxK (22), PxxPxR (32), and RxxK (23), with the exception of MONA-8. One of the isolated peptides, MONA-4, shared four identities with the P2 peptide, three of which are present in the P2-binding motif (PxxxRxxKP), and four additional similarities. The highest-affinity ligands, MONA-1 and MONA-2, combined both the class II and class III (RxxK, 3^{10} helix) motifs (31) and shared a consensus of PxxPxRxxK. MONA-5 contained the core-binding motif PxxP. Thus, all but one of the Mona ligands identified by FRET hybrids possessed a motif known to be physiologically relevant.

The consensus among PDZ2-binding peptide ligands was similarly striking. Remarkably, all ligands having dissociation constants <1 μM possessed a PDZ domain recognition sequence S/TxV-COOH (30), and many exhibited a strong preference for tryptophan at the -3 position (Table 1). Among 18 unique ligands, apparent dissociation constants ranged from 0.1 μM to >1 μM. Peptides terminating with residues L, I, C, and P occurred infrequently and possessed higher K_D values than those with a terminal valine, consistent with the fact that PDZ2 binds peptides terminating in leucine and isoleucine with low affinity (30). Several of the isolated PDZ2-binding peptides exhibited higher affinity than the known ligands NR2 and Cript [the C-terminal sequence of the protein known as cysteine-rich interactor of PDZ three (CRIPT); ref. 33]. One peptide exhibiting high affinity in this assay [PDZ2–2 (NTSV-COOH); K_D = 110 nM] shared three C-terminal identities and one similarity with the Cript ligand (KQTSV-COOH).

Given the potential value of screening protein–peptide interactions in a wider variety of cellular contexts by using high-throughput cell-sorting instrumentation, we measured the dynamic range afforded by FACS for FRET-hybrid interactions taking place in the cytoplasm of both yeast and mammalian cells. Intracellular expression of FRET hybrids in *E. coli* provided sufficient, albeit overlapping (Fig. 4*A*), FRET signals to enable screening for protein interactions by using sequential enrichment by FACS. In contrast, coexpression of the interacting hybrids YPet-Mona and CyPet-P2 in *Saccharomyces cerevisiae* and human embryonic kidney cells (293T) resulted in ratiometric FRET signal dynamic ranges improved by >2-fold in yeast and 3-fold in 293T cells (Fig. 4 *B* and *C*) relative to those measured for bacterial cells by using flow cytometry. Cells expressing interacting partners exhibited FRET signals that were clearly resolvable from those expressing noninteracting partners, suggesting that libraries could be efficiently screened for protein–ligand interactions in yeast or animal cells with fewer rounds of cell sorting.

Discussion

Both yeast (2, 9) and bacterial two-hybrid systems (34) rely on signal amplification that occurs when receptor–ligand interactions initiate transcriptional activation and reporter gene expression (35). Whereas signal amplification provides high sensitivity to detect even weak interactions (35), two-hybrid systems can yield a high frequency of false-positive interactions (9). Furthermore, approaches that rely on transcriptional activation report the cumulative ensemble average of interactions occurring over an extended period, typically hours. Consequently, they are not amenable to screening for reversible or dynamic phenomena. Given the limitations of two-hybrid assays, protein fragment complementation has been pursued as a means to directly report interactions without a requirement for secondary events (36, 37) and may prove useful for large-scale interaction screening (36, 38). In this report, FRET hybrids enabled direct quantitative and near-real-time detection of protein–ligand interactions in bacteria, yeast, and mammalian cells and a means to rapidly measure binding affinity. Reversible binding of FRET hybrids enabled high-throughput measurement of binding constants to quantitatively score interaction partners isolated from a library. The ability to rank affinity in a high-throughput manner by using FRET hybrids is unique among protein-interaction assays and provides a valuable tool for interaction-mapping experiments.

The application of genetically encoded FRET probes for protein-interaction screening offers exciting possibilities for large-scale, quantitative interaction mapping and dynamical studies of protein networks. Unlike two-hybrid or complementation screens, FRET hybrids do not require secondary binding events or physical interactions between probes. However, for detection, protein-interaction partners must bring their respective probes to within an appropriate distance (≈5–10 nm) and orientation compatible with FRET. These two parameters likely were responsible for the variation in maximal FRET signals observed for different ligands isolated in this study. Although flexible linkers may circumvent the orientation problem, interactions between larger proteins may not be detectable, because the FRET probes may remain separated by >10 nm. Construction of libraries as both N- and C-terminal fusions with fluorescent proteins may help to alleviate distance constraints in some cases. Alternatively, the use of protein domains derived from cDNA fragment libraries in interaction screens could mitigate this problem. In the present study, domain-level screening provided a means to precisely map the binding epitopes in a manner that would not have been possible with full-length proteins, because the discovered ligands otherwise could not be directly mapped to particular domains of the target protein.

FRET hybrids enabled unambiguous identification of the ligand preferences of two different types of protein-interaction modules. The C-terminal SH3 domain of Mona, a scaffolding protein involved in hematopoietic signaling, is known to recognize proline-rich sequences containing the PxxP motif and was originally discovered in a yeast two-hybrid screen against Fms, a tyrosine kinase receptor of macrophage-colony stimulating factor (21). In the present study, seven of eight identified ligands incorporated binding motifs known to be physiologically relevant. Whereas all but one Mona-SH3 binding ligands had PxxP or RxxK motifs, FRET hybrids also identified higher affinity ligands (K_D ≈100 nM) that combined the above two motifs into a single-sequence (PxxPxRxxKxR/K). Interestingly, this "combination motif" occurs within the Mona ligand, hematopoietic progenitor kinase-1 (HPK1) (24), and MONA-1 shared seven identities of the core-binding motif with HPK1.

The second PDZ domain of postsynaptic protein PSD-95 is known to interact with a subunit (NR2) of NMDA receptors in dendrites (29) and is involved in memory and learning (39). The ligand preferences of this PDZ domain have been investigated with individually synthesized peptides, revealing a strong preference for S/TxV-COOH and, more rarely, leucine or isoleucine at the 0 position (30). An identical ligand preference was

identified with FRET hybrids. Four C-terminal residues of the ligand PDZ2-3 (STVV-COOH) identified in the current study with FRET hybrids are identical to those from the NR1 subunit of NMDA receptor, although Y2H assays have not identified this interaction (40). Finally, short peptides derived from the C terminus of NMDA receptor (NR2) have been shown to prevent neuronal death after stroke in a rat model (41). Using FRET hybrids, several ligands were identified that bound PDZ2 with higher affinity than the peptide derived from NR2, suggesting that this approach could enable discovery of therapeutically useful protein-interaction inhibitors (42).

Because yeast and bacterial hybrid systems do not enable direct quantitative determination of dissociation constants, affinity measurements can be rate limiting in high-throughput interaction studies. FRET hybrids enabled high-throughput measurement of dissociation constants in the presence of complex protein mixtures. The use of FRET hybrids in the presence of complex physiological protein mixtures may provide a means to more accurately assess effective binding affinities. The ability to rapidly discover protein–domain interaction partners and determine their binding affinity with FRET may prove useful for generating quantitative interactome maps that can be translated into network models of cell function.

Considering that fluorescent proteins are functional in a variety of cell types and compartments (43), FRET hybrids should be extendable to a broad range of host cells. We applied *E. coli* as an expression host for library screening, given its rapid growth rate, high transformation efficiency, and ease of manipulation. However, FRET hybrids in the cytoplasm of yeast and mammalian cells yielded substantial improvements in the FRET-dynamic range, enabling efficient high-throughput screening of interaction partners by using FACS. The ability to screen intracellular protein interactions within a more diverse group of cell types will enable screening in the environment that is most relevant to the interaction of interest.

Materials and Methods

Plasmid and Library Construction. Vectors encoding YPet-Mona and CyPet-peptide fusions were constructed for separate expression of each binding partner. To improve library construction efficiency, a stuffer sequence containing a kanamycin (Kan) resistance gene flanked by two SfiI sites was inserted into pBAD33 (44), generating pB33Kan. The murine C-terminal SH3 domain of Mona (22) was constructed by gene assembly (45). YPet and Mona coding sequences were joined by overlap PCR creating a gene-encoding YPet-GGSPRG-Mona (or YM). This YM PCR product was digested and ligated to the SfiI site of pB33Kan, resulting in pB33YM. The gene-encoding CyPet was amplified by primers that encoded a GGSPRG linker, and the "P2 ligand" (PAPSIDRSTKPPL), followed by a SfiI restriction site. pB33CyPet-P2 (or pB33CyP2) was created similarly.

Bicistronic vectors were constructed for coexpression of YPet-Mona and CyPet-P2 (or CyPet alone as a negative control) in bacteria. PCR fragments encoding YPet-Mona and CyPet-P2 or CyPet were joined by overlap PCR and ligated into SfiI-digested pB33Kan, yielding pB33YM-CyP2 and pB33YM-CyPet. Similarly, bicistronic expression vectors were constructed encoding YPet-PDZ2 (YP) and CyPet-peptide fusions. The gene encoding the PDZ2 domain of PSD-95 (amino acids A198–A292) (28) was a generous gift from Ken Kosik (University of California, Santa Barbara). CyPet was amplified with primer 1 and two nested reverse primers 2 and 3 (see Table 2, which is published as supporting information on the PNAS web site). This PCR yielded a gene encoding the fusion CyPet-GGSGSGIESDV (CyPet-NR2). Vectors encoding CyPet-GGSGSGKQTSV (CyPet-Cript) and CyPet-GGSGSGSESKE (CyPet-SESKE) were similarly created. For library construction, CyPet was amplified with a forward primer upstream of the start codon and the reverse primer 5′-cagccaagcttggccaccttggcctta$(SNN)_{15}$tcccctaggg ctaccacctttgtacaat-3′ (where N = A/C/G/T and S = C/G), generating a gene-encoding CyPet with a GGSPRG linker sequence followed by a 15-mer random peptide library (CyLib). The CyLib PCR product and pB33YM/CyPet were cut with XbaI and HindIII and ligated, resulting in the pB33YM/CyLib library. The plasmid library was transformed to MC1061 *E. coli*, producing 2×10^6 transformants in total. A similar strategy was used to create pB33YP/CyLib.

***In Vitro* FRET Measurements.** *E. coli* MC1061 cells were grown overnight at 37°C in LB medium, supplemented with 34 μg/ml chloramphenicol. Cultures were diluted 1:100, incubated at 37°C for 2 h and induced with 0.2% wt/vol L-(+)-arabinose at 22°C for 6 h. Cell lysates were prepared with B-PER II Bacterial Protein Extraction Reagent (Pierce, Rockford, IL) by following the manufacturers' protocol. The fluorescent protein fusion concentrations were determined by using Beer's law. Lysates from interacting partners, YM and CyP2, were mixed at a 1:0.7 molar ratio and diluted to 12 different concentrations in PBS (pH 7.4). Mixtures of YM with CyPet, YPet with CyP2, and YPet with CyPet were similarly prepared. Emission intensities of each mixture were scanned between 460 nm and 560 nm with 414 nm excitation, and the FRET ratio was defined as the ratio of 527:475 nm emission. For relative intensity measurements (Fig. 2*A*), the spectra were divided by the maximum emission intensity of the YM-CyP2 positive control.

Determination of Optimal Induction Conditions for *in Vivo* FRET. Cells transformed with the bicistronic vectors pB33YM/CyP2 or pB33YM/CyPet were cultured overnight and diluted 1:100 into fresh medium. Expression was induced with 0.2% L-(+)-arabinose for a period of 1–6 h. The cells then were pelleted by centrifugation at $2,700 \times g$ for 5 min, resuspended in PBS, and incubated with shaking for an additional 1–5 h, such that the combined incubation time after inducer addition was 6 h in each case. For example, for the 1-h time point, the culture was induced for 1 h, and incubated in PBS for 5 h. Control samples were analyzed by using the FACSAria (BD Biosciences) flow cytometer, with 407-nm excitation. Entirely nonfluorescent particles were excluded from FRET analysis by pregating on yellow emission (530/30 nm) with 488-nm excitation.

FRET Hybrids Library Screening. For the isolation of both Mona and PDZ2-binding peptides, protein expression was induced for 2 h with 0.2% L-(+)-arabinose at 22°C, cells were spun down at $2,700 \times g$ for 5 min, resuspended in PBS (pH 7.4), and allowed to shake at 22°C for an additional 4 h. Four rounds of FACS, using a FACSAria flow cytometer (BD Biosciences), were used to isolate clones exhibiting high FRET. The cyan (450/40 nm) and yellow (530/30 nm) fluorescence intensities with violet excitation (407 nm) were collected. Those cells exhibiting a high yellow to cyan fluorescence ratio were sorted into SOC medium and grown overnight for further rounds of screening. Cells from the final round of sorting were plated and picked for individual analysis in 96-well plates by using a Safire (Tecan) fluorescence spectrophotometer. Selected clones were characterized by DNA sequencing and their dissociation constants were determined.

Measurement of Affinity by Using FRET. To determine the K_D of YPet–SH3/PDZ and CyPet–peptide interactions, fusions were coexpressed from bicistronic vectors overnight at 22°C. The cell lysates were prepared as described above. YPet–SH3/PDZ concentrations in lysates were determined by using a calibration curve (data not shown) of fluorescence intensity as a function of YPet concentration in lysate. Samples were serially diluted over approximately three orders of magnitude, and the emission ratio of 527:475 nm (FRET ratio) with CyPet excitation was mea-

sured. The resulting equilibrium curves were fit to an equilibrium-binding equation to determine the K_D (*Supporting Text*, which is published as supporting information on the PNAS web site).

Mammalian Cell Expression and FACS Analysis. To coexpress YPet-Mona and CyPet-P2 in human embryonic kidney cells (HEK and 293T), the respective genes were subcloned into a bicistronic retroviral expression vector (pQCXIX) by using an internal ribosome entry site (BD Biosciences). Genes encoding YPet-Mona with mammalian optimized codons were amplified by using primers 4 and 5 (Table 2). CyPet-P2- and CyPet-encoding genes, with mammalian-optimized codons, were amplified with primers 6–9 (Table 2). The resulting YPet-Mona-encoding gene was digested with EcoRI and NotI, CyPet-P2- and CyPet-encoding genes were digested with MluI and XhoI and ligated with similar digested pQCXIX, yielding pQYM/CyP2 and pQYM/CyPet. The pQYM/CyP2 (positive control) or pQYM/CyPet (negative control) plasmids were mixed with pQCXIX (blank) plasmid at a 1:20 ratio of positive or negative to blank plasmid. 293T cells were transfected with the mixture by calcium phosphate precipitation (46). Transfected 293T cells were maintained in DMEM with 10% FBS. Cells were harvested and analyzed by FACS as described above 72 h after transfection.

Yeast Expression and FACS Analysis. Yeast strains were constructed with chromosomally integrated genes encoding CyPet and YPet or CyPet-P2 and YPet-Mona. The 2-μm origin was removed from the pYES2NT and pYES3NT plasmids (Invitrogen) by digestion with NgoMIV and ClaI. Klenow polymerase then was used to fill in the 5′ overhangs, and the vector again was ligated. CyPet, YPet, CyPet-P2, and YPet-Mona then were cloned between the KpnI and NotI sites in these plasmids. The CyPet- and YPet-encoding genes were integrated into the yeast JYL69 (MATa *ura*3-1 ADE2+ *his*3-11,15 *leu*2-3,112 *trp*1-1 *can*1-100; isogenic to W303) genome by using the high-efficiency PEG/lithium acetate method (47). Cells were grown for 24 h in yeast peptone medium supplemented with 2% raffinose at 22°C. Cultures were diluted to 1:100 for overnight, induced with 2% G-galactose for 7 h, and analyzed by FACS.

We thank Y. Zhu, K. Dane, and P. Bessette for critically reading the manuscript. This work was supported by National Institutes of Health–National Institute of Biomedical Imaging and Bioengineering Grant EB-000205, National Science Foundation (NSF)-CAREER Award BES-0449399, and an NSF graduate fellowship (to A.W.N.).

1. Cagney G, Uetz P, Fields S (2000) *Methods Enzymol* 328:3–14.
2. Fields S, Sternglanz R (1994) *Trends Genet* 10:286–292.
3. Schwikowski B, Uetz P, Fields S (2000) *Nat Biotechnol* 18:1257–1261.
4. Uetz P, Giot L, Cagney G, Mansfield TA, Judson RS, Knight JR, Lockshon D, Narayan V, Srinivasan M, Pochart P, *et al.* (2000) *Nature* 403:623–627.
5. Davy A, Bello P, Thierry-Mieg N, Vaglio P, Hitti J, Doucette-Stamm L, Thierry-Mieg D, Reboul J, Boulton S, Walhout AJ, *et al.* (2001) *EMBO Rep* 2:821–828.
6. Giot L, Bader JS, Brouwer C, Chaudhuri A, Kuang B, Li Y, Hao YL, Ooi CE, Godwin B, Vitols E, *et al.* (2003) *Science* 302:1727–1736.
7. Rual JF, Venkatesan K, Hao T, Hirozane-Kishikawa T, Dricot A, Li N, Berriz GF, Gibbons FD, Dreze M, *et al.* (2005) *Nature* 437:1173–1178.
8. Farmer TB, Caprioli RM (1998) *J Mass Spectrom* 33:697–704.
9. Fields S (2005) *FEBS J* 272:5391–5399.
10. Michnick SW (2004) *Drug Discov Today* 9:262–267.
11. Houtman JC, Barda-Saad M, Samelson LE (2005) *FEBS J* 272:5426–5435.
12. Drewes G, Bouwmeester T (2003) *Curr Opin Cell Biol* 15:199–205.
13. Pawson T, Nash P (2003) *Science* 300:445–452.
14. Ambasta RK, Kumar P, Griendling KK, Schmidt HH, Busse R, Brandes RP (2004) *J Biol Chem* 279:45935–45941.
15. Camuzeaux B, Spriet C, Heliot L, Coll J, Duterque-Coquillaud M (2005) *Biochem Biophys Res Commun* 332:1107–1114.
16. Collinson AD, Bligh SW, Graham DL, Mott HR, Chalk PA, Korniotis N, Lowe PN (2004) *Assay Drug Dev Technol* 2:659–673.
17. Clegg RM (2002) *J Biotechnol* 82:177–179.
18. Aoki K, Nakamura T, Matsuda M (2004) *J Biol Chem* 279:713–719.
19. Rizzo MA, Springer GH, Granada B, Piston DW (2004) *Nat Biotechnol* 22:445–449.
20. Nguyen AW, Daugherty PS (2005) *Nat Biotechnol* 23:355–360.
21. Bourette RP, Arnaud S, Myles GM, Blanchet JP, Rohrschneider LR, Mouchiroud G (1998) *EMBO J* 17:7273–7281.
22. Harkiolaki M, Lewitzky M, Gilbert RJ, Jones EY, Bourette RP, Mouchiroud G, Sondermann H, Moarefi I, Feller SM (2003) *EMBO J* 22:2571–2582.
23. Berry DM, Nash P, Liu SK, Pawson T, McGlade CJ (2002) *Curr Biol* 12:1336–1341.
24. Lewitzky M, Harkiolaki M, Domart MC, Jones EY, Feller SM (2004) *J Biol Chem* 279:28724–28732.
25. Derdowski A, Ding L, Spearman P (2004) *J Virol* 78:1230–1242.
26. Kretzschmar AK, Dinger MC, Henze C, Brocke-Heidrich K, Horn F (2004) *Biochem J* 377:289–297.
27. Mahajan NP, Linder K, Berry G, Gordon GW, Heim R, Herman B (1998) *Nat Biotechnol* 16:547–552.
28. Stathakis DG, Hoover KB, You Z, Bryant PJ (1997) *Genomics* 44:71–82.
29. Kornau HC, Schenker LT, Kennedy MB, Seeburg PH (1995) *Science* 269:1737–1740.
30. Lim IA, Hall DD, Hell JW (2002) *J Biol Chem* 277:21697–21711.
31. Li SS (2005) *Biochem J* 390:641–653.
32. Sparks AB, Rider JE, Hoffman NG, Fowlkes DM, Quillam LA, Kay BK (1996) *Proc Natl Acad Sci USA* 93:1540–1544.
33. Niethammer M, Valtschanoff JG, Kapoor TM, Allison DW, Weinberg TM, Craig AM, Sheng M (1998) *Neuron* 20:693–707.
34. Joung JK, Ramm EI, Pabo CO (2000) *Proc Natl Acad Sci USA* 97:7382–7387.
35. Van Criekinge W, Beyaert R (1999) *Biol Proced Online* 2:1–38.
36. Remy I, Michnick SW (2004) *Methods* 32:381–388.
37. Hu CD, Kerppola TK (2003) *Nat Biotechnol* 21:539–545.
38. Remy I, Michnick SW (2004) *Methods Mol Biol* 261:411–426.
39. El-Husseini AE, Schnell E, Chetkovich DM, Nicoll RA, Bredt DS (2000) *Science* 290:1364–1368.
40. Bassand P, Bernard A, Rafiki A, Gayet D, Khrestchatisky M (1999) *Eur J Neurosci* 11:2031–2043.
41. Aarts M, Liu Y, Liu L, Besshoh S, Arundine M, Gurd JW, Wang YT, Salter MW, Tymianski M (2002) *Science* 298:846–850.
42. Geyer CR, Brent R (2000) *Methods Enzymol* 328:171–208.
43. Zhang J, Campbell RE, Ting AY, Tsien RY (2002) *Nat Rev Mol Cell Biol* 3:906–918.
44. Guzman LM, Belin D, Carson MJ, Beckwith J (1995) *J Bacteriol* 177:4121–4130.
45. Stemmer WP, Crameri A, Ha KD, Brennan TM, Heyneker HL (1995) *Gene* 164:49–53.
46. Miller AD, Rosman GJ (1989) *Biotechniques* 7:980–990.
47. Gietz RD, Woods RA (2002) *Methods Enzymol* 350:87–96.